Chapter 2
Experimental Details and Developments

2.1 Introduction

This chapter describes the experimental setup and it's related components that were used in the present thesis work. We have performed extensive measurements on single ionization of several gaseous targets and biomolecules induced by different projectiles. For this purpose, the electron spectroscopy technique was used to measure the ionized electrons. The experiments were performed with an electron gun and with the two accelerators at TIFR, i.e., the TIFR-ECR ion accelerator and the 14 MV BARC-TIFR Pelletron accelerator. The electron gun is capable of generating keV energy electrons. The ECR ion accelerator provides low energy highly charged ions whereas the Pelletron accelerator generates MeV energy ions. The projectiles used were 3 to 8 keV electrons, 150 and 200 keV protons and 42 and 66 MeV bare C ions. The keV energy protons were obtained from the electron cyclotron resonance based ion accelerator (ECRIA) facility at TIFR, Mumbai. Bare C ions of energies 3.5 MeV/u and 5.5 MeV/u were available from the 14 MV TIFR-BARC Pelletron accelerator facility at TIFR, Mumbai. The keV energy electron impact ionization studies were performed for two di-atomic molecules N_2 and O_2. Gaseous targets, He, CH_4 and O_2 were bombarded with keV energy protons, whereas for O_2 experiments were also performed in collision with 5.5 MeV/u C^{6+} ions. Biomolecular targets, uracil ($C_4H_4N_2O_2$) and bromouracil ($C_4H_3BrN_2O_2$) were ionized using 200 keV protons and MeV energy C^{6+} ions. For all the experiments, the absolute DDCS for electron emission were measured and thereafter several information were extracted from the measured quantities.

2.2 Experimental setup

Our experimental arrangement can be divided in five main parts: $1)$ projectile: generated from the electron gun, the ECR ion accelerator and Pelletron accelerator, $2)$ scattering chamber, $3)$ target from effusive jet source, $4)$ electron spectrometer and $5)$ detector.

2.2.1 ECR-Ion accelerator

Electron cyclotron resonance (ECR) ion accelerators are suitable for generating low velocity highly charged ions with very high current. The ECR ion source used for the present series of experiments is a "Super nanogan" designed and manufactured by Ms Pantechnik, France. This is a 14.5 GHz machine with a maximum extraction voltage of 30 kV. The positively charged

ions are produced inside the ion source which is confined within strong magnetic field satisfying the *"minimum-B"* configuration. This implies that the absolute value of the magnetic field has a minimum at the center of the ion source and increases in all directions as one moves towards the boundaries. The ions are extracted by applying an extraction voltage of maximum 30 kV and then a 90^0 bending dipole magnet is used to select the desired ions. The plasma chamber, Einzel lens and the bending magnet are all placed together on an isolated high voltage (HV) deck which can be raised upto 400 kV [54, 55]. The analyzing magnet is followed by an accelerating column, one end of which is at the HV deck potential while it's other end is at ground potential, thus accelerating the charge state selected ions to the required energy. Electrostatic triplet quadrupole lenses and electrostatic X-Y deflectors are used to focus the energy and charge state analyzed projectile beam. The ECRIA has four beamlines and a switching magnet is used to steer the beam in the desired beamline. The electron spectroscopy assembly is connected to the 50^0 N beamline. The beamline is equipped with electrostatic quadrupole triplet lenses and several X-Y deflectors for focussing and steering the ion beam. A pair of four jawed slits are also used to cut the beam and control the beam divergence. Further, three Faraday Cups are placed at different points over the entire beamline (i.e., between the ion source and the end of the beamline) to measure the ion beam current. A differential pumping arrangement was connected at the end of the beamline which was followed by the scattering chamber. An extended aperture of diameter 2 mm and length 30 mm was placed at the end of the beamline (at the junction between the beamline and the differential chamber) and another aperture of 4mm diameter was placed just at the entrance of the scattering chamber for further beam collimation. A high vacuum isolation valve is connected at the end of each beamline which helps to isolate the beamline from the experimental setup (whenever required). The entire beamline along with the switching magnet was re-aligned with respect to the ion source. The alignment was done initially with water mark and then was fine tuned by aligning with laser beam. 150 keV and 200 keV proton beams were used for the present experiments using this accelerator. The beamline pressure was maintained at about $5x10^{-9}$ mbar at all times. It is necessary to maintain a high vacuum in the beamline to reduce the probability of charge neutralization of the projectile ions. Several sets of turbo molecular pumps (TMPs) backed by rotary pumps are used to maintain the high vacuum in the accelerating column and all the beamlines. The entire beamline is made of non-magnetic stainless steel.

2.2.2 Pelletron beamline

The experiments involving MeV energy highly charged ions were performed using the 14 MV BARC-TIFR Pelletron accelerator facility. The energy and charge state analysed C^{4+} ions were passed through a post-stripper carbon foil arrangement to obtain ions of higher charge state including bare ions. The C^{6+} ions were selected using a switching magnet and directed to the desired beamline. The present experiments were performed at the 30^0 south beamline. A

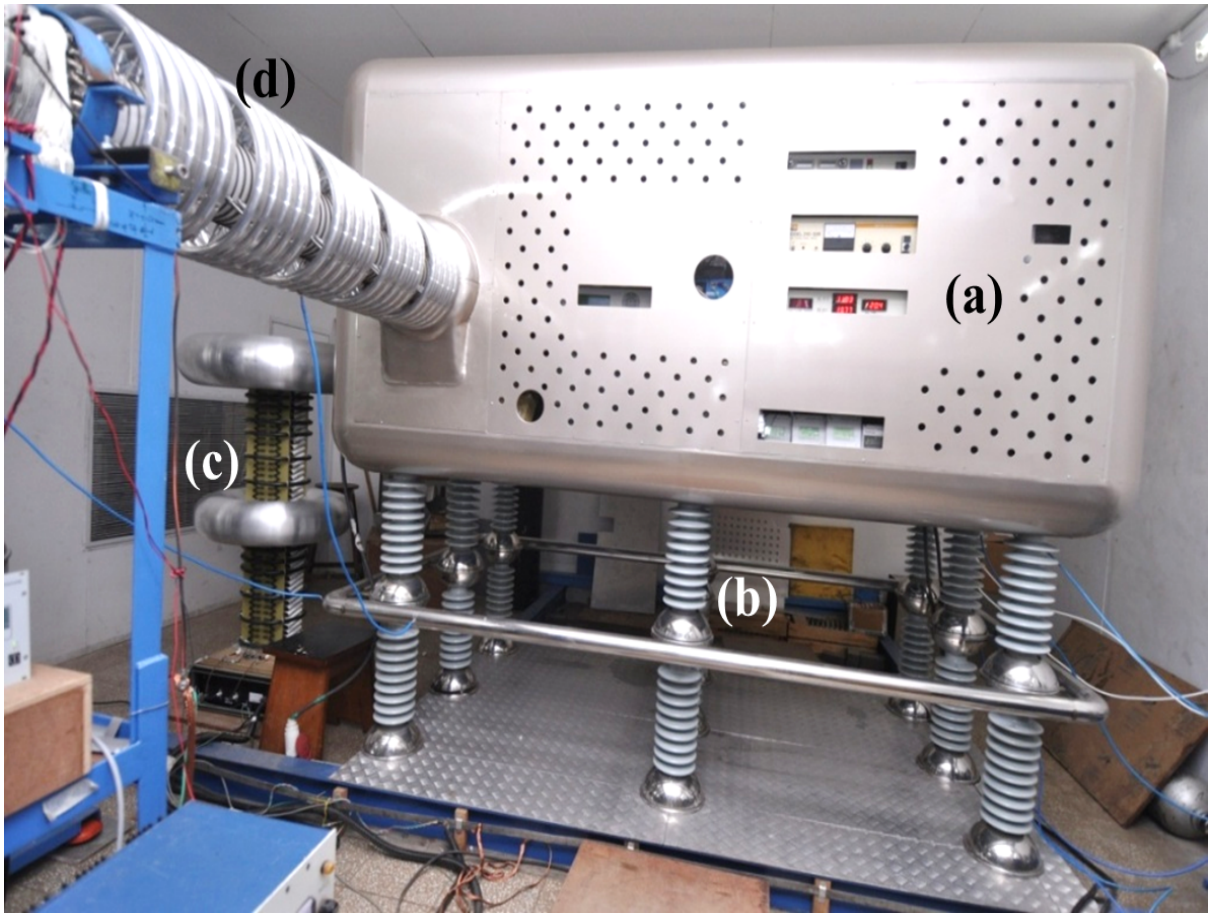

Figure 2.1: ECR ion accelerator showing (a) high voltage (HV) deck, (b) ceramic insulators (c) high voltage power supply (d) accelerating column.

pair of four-jawed slits, mounted 1 m apart was used to cut the beam to the desired size. This was followed by another aperture of diameter 4 mm. Successive collimation of the ion beam leads to the production of well collimated parallel electron beam with almost no divergence. A pneumatic valve is connected at the end of the beamline which is followed by the differential pumping arrangement and the main scattering chamber.

2.2.3 Beamline for electron gun

The keV energy electron beams were produced from a commercially available electron gun (Kimball EGPS-3101B). The energy of the electrons were varied between 3 and 8 keV for the experimental studies. The electrons emitted from the cathode due to thermionic emission were initially focussed with a set of Einzel lens and electrostatic deflectors which were customized with the electron gun assembly. However, electron being a light mass particle gets easily deflected. The distance between the electron gun filament and interaction region in the scattering chamber being quite large, about 1.5 m, one set of lens and deflectors was not sufficient to get a well-collimated parallel beam near the interaction region. Thus another set of Einzel lens,

X-Y deflectors and several apertures of varying dimensions were incorporated in the beamline to focus the beam properly. These apertures were used to cut the beam at various stage and to reduce the probability of forward moving electrons generated from slit scattering to reach near the interaction region which could lead to enormous background counts at the extreme forward angles. All the beam optics elements placed at different locations in the beamline were required to produce a collimated parallel electron beam. The entire beamline was revamped and realigned to improve the beam quality and beam transmission for performing the present experiments. The electron gun filament was aligned under high vacuum condition with respect to the anode aperture and further apertures in the beamline. This exercise improved the beam current drastically from tens of nA to several hundreds of nA. Further, two pairs of magnetic coils were also incorporated in the beamline (shown in Figure 2.3). This helped to increase the beam transmission to a large extent from 70% to 90%. The typical beam current was $\sim$ 900 nA which remained stable over the entire experimental process. Figure 2.2 shows the second set of Einzel lens, electrostatic deflectors and several collimators which were made as an independent assembly and this assembly was connected to the differential pumping arrangement, just preceding the scattering chamber.

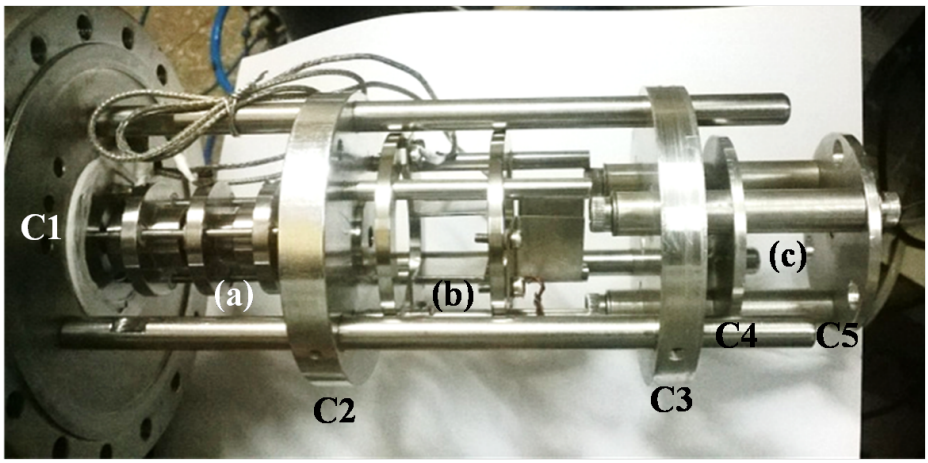

Figure 2.2: Picture of different beam optics elements (a) Einzel lens, (b) X-Y deflectors, (C1 to C5) apertures of various dimensions.

2.2.4 Scattering chamber

Figure 2.3 displays the 3D diagram of the high vacuum scattering chamber along with the beamline for electron gun assembly. The scattering chamber is a stainless steel tube of diameter 18 inch. A base pressure of 5 x 10^{-8} mbar was achieved with a 3000 l/sec turbo molecular pump backed by a 600 l/sec tri-scroll pump. The tri-scroll pumps are oil free, which was required for the detection of low energy electrons ($\leq$ 5 eV). The scattering chamber has eight side ports which were required for various purposes, e.g., gas inlet, vacuum gauge, vacuum compatible feed through for electrical connections, Faraday Cup, MKS Baratron etc. The scat-

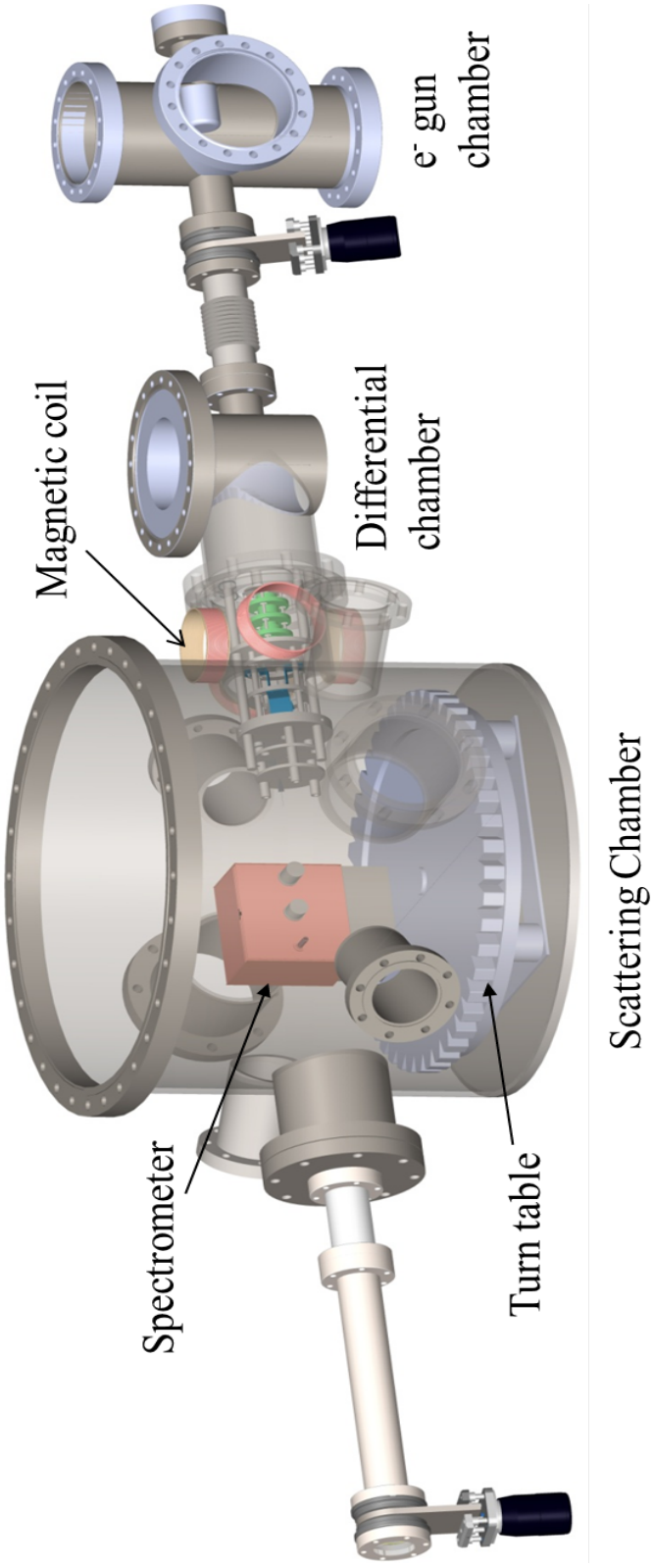

Figure 2.3: 3-D mechanical drawing of the scattering chamber housing the turntable spectrometer, differential assembly along with the focussing elements and the electron gun chamber housing the electron gun (made using SolidWorks-2014). Three turbo pumping stations attached with these three chambers are not shown.

tering chamber was flooded with the target gas at a suitable gas pressure so as to maintain single collision condition. For certain experiments the absolute gas pressure was maintained at 0.1 mTorr whereas for others it was at 0.15 mTorr. The absolute pressure of the target gas was measured using a capacitance manometer (MKS Baratron). High purity nitrogen, oxygen, helium, methane gases were used as targets for the experiments. For certain cases, an effusive gas jet was also used. In the case of the effusive jet source, the experiment was performed in a crossed-beam arrangement. For either cases, the flow of the gas inside the scattering chamber was controlled using a solenoid valve. The differential pumping assembly, which was connected between the scattering chamber and the beamline for all the experiments was required to maintain the pressure difference between the two, particularly being important for experiments where the scattering chamber was flooded with the target gas. It was necessary to maintain extreme cleanliness inside the chamber and any exposed insulating surfaces were properly covered with aluminium foils and grounded so as to avoid any kind of static charge development on such surfaces. The Earth's magnetic field was reduced to about 5–10 mGauss near the interaction region by placing two sets of thin μ metal sheets (thickness $\sim$ 0.3 mm) on the inner side of the scattering chamber. The scattering chamber houses a motorized turntable on which there is a base plate and the spectrometer sits on the base plate. In Figure 2.3 one can see the turntable along with the base plate and the spectrometer. A stepper motor driven, bellow sealed, rotary vacuum feed-through was used to rotate the turn table. Each rotation of the stepper motor rotates the turn table by 3.3^0. The rotation of the turn table was controlled externally by interfacing the motor with a computer through a LabVIEW based program.

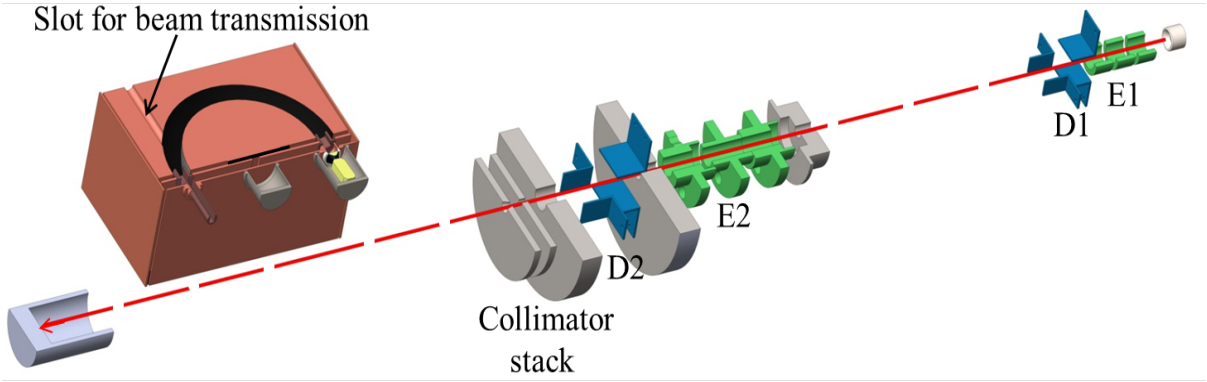

Figure 2.4: 3-D mechanical drawing of the magnified, cross sectional view of the beamline components (not to scale) along with the spectrometer and Faraday Cup. E1 and D1 are the Einzel lens and electrostatic deflectors, respectively, mounted in the e-gun assembly; similarly, another set of Einzel lens (E2) and deflectors (D2) are mounted in the beamline. Several apertures, placed at different points along the beamline are also shown, (made using SolidWorks-2014).

Figure 2.4 shows the cross sectional view of the focussing elements used for focussing of electron beam, spectrometer and the Faraday Cup alongwith a typical projectile beam direction.

Figure 2.4 shows a magnified view of all the elements and hence is not to scale. The incident beam was collected on the Faraday Cup for beam normalization purpose. The Faraday Cup was electrically isolated from the main scattering chamber. It was kept sufficiently long in order to prohibit the back scattered electrons from reaching the interaction region. The projectile beam transmission was obtained by comparing the beam current from two positions of the spectrometer, i.e. aligned along 0^0 and then by moving it away from the beam path. When the spectrometer is placed in-line with the beam direction, the projectile beam has to pass through the slot on the outer hemisphere (shown in Figure 2.4). In such situation, the beam has to pass through several (i.e. five) apertures on the spectrometer, apart from the ones used for beam collimation, before falling on the Faraday cup. For all the experiments, the beam transmission was about 85-90%. It was important to achieve a high transmission after following the stringent beam path, ensuring a well collimated parallel beam. Otherwise, a diverging beam (i.e., poor beam transmission) would result in high background counts at the extreme forward angles due to beam scattering at the surface of the spectrometer or with other components in the beamline.

The scattering chamber described so far was connected to the electron gun assembly and Pelletron accelerator beamline for performing experiments with electron beam and MeV energy highly charged ions. Another scattering chamber, identical to the above mentioned one was connected to the 50^0 north beamline of the ECR ion accelerator for executing experiments with keV energy protons. In this scattering chamber, each rotation of the stepper motor rotates the turn table by 2.5^0.

2.2.5 Effusive jet and oven assembly

An effusive jet source made from non-magnetic stainless steel was used to perform experiment with gaseous target, O_2 in collision with 200 keV protons from the ECR ion accelerator. The nozzle of diameter 1 mm and length 10 mm (aspect ratio 0.1) was used as the effusive gas inlet inside the scattering chamber. A solenoid valve was used to control the flow of O_2 through the jet inlet. The projectile ions and the effusive gas-jet target cross each other at right angles within the interaction region. The tip of the nozzle was kept 5 mm above the beamline. The jet source was connected to a below sealed 3D translation stage manipulator for proper alignment of target gas with the beam. Initially, mechanical alignment was performed to align the jet nozzle with the beamline and the plane of the spectrometer. For this purpose, the nozzle was aligned with respect to the aperture placed at the entrance of the scattering chamber and with the collimator of the spectrometer. Further, to ensure an accurate overlap of the target jet profile with the projectile beam, the count rate was checked by moving the jet nozzle perpendicular to the beamline. Figure 2.5 displays the change in count rate which was recorded for two different electron emission energies. In the figure, 0 represents the position obtained from mechanical alignment. The data were collected every time when moving the nozzle by 0.5 mm and then the nozzle position was finalized for the maximum count rate. During the experiment, the jet

backing pressure was maintained at 100 mTorr which resulted in a base pressure of 1.7 x 10^{-6} mbar inside the scattering chamber.

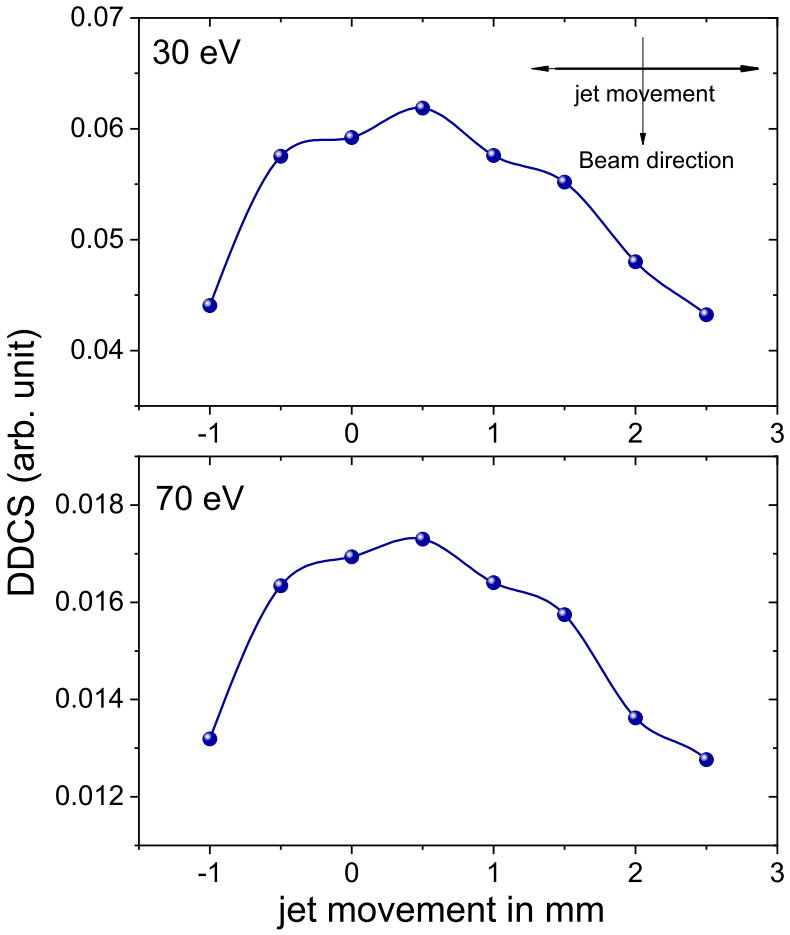

Figure 2.5: Count rate as a function of jet nozzle movement with respect to the projectile beam. The effusive jet nozzle is moved perpendicular to the beam direction.

In case of targets like uracil and bromouracil, which are available in powder form, an oven assembly was prepared to produce the vapour of the targets. Figure 2.6 shows the 3D drawing of the oven assembly. The commercially available powder of bromouracil (99.8% pure) was placed in a cylinder made of oxygen free high conductivity (OFHC) copper having diameter 5 mm and height 30 mm. This cylinder, containing the target powder sample was placed inside the metallic oven. A nozzle made of OFHC copper of aspect ratio (diameter/length) 0.1 was placed on top of the oven to obtain effusive molecular beam of vapourized bromouracil. The oven temperature was monitored by a thermocouple temperature sensor coupled to the heater body. The temperature of the oven was maintained at around 140 - 200 ^{0}C during the experiment. The cross sectional view of the oven is shown in Figure 2.8, showing all the internal parts of the oven along with the cylinder containing the powder and the nozzle. During the measurements, the heat transfer from the oven to the electron detector on the spectrometer can give rise to the generation of dark counts. To avoid the production of dark counts, the oven was

mounted inside a water cooled jacket (shown in Figure 2.6).

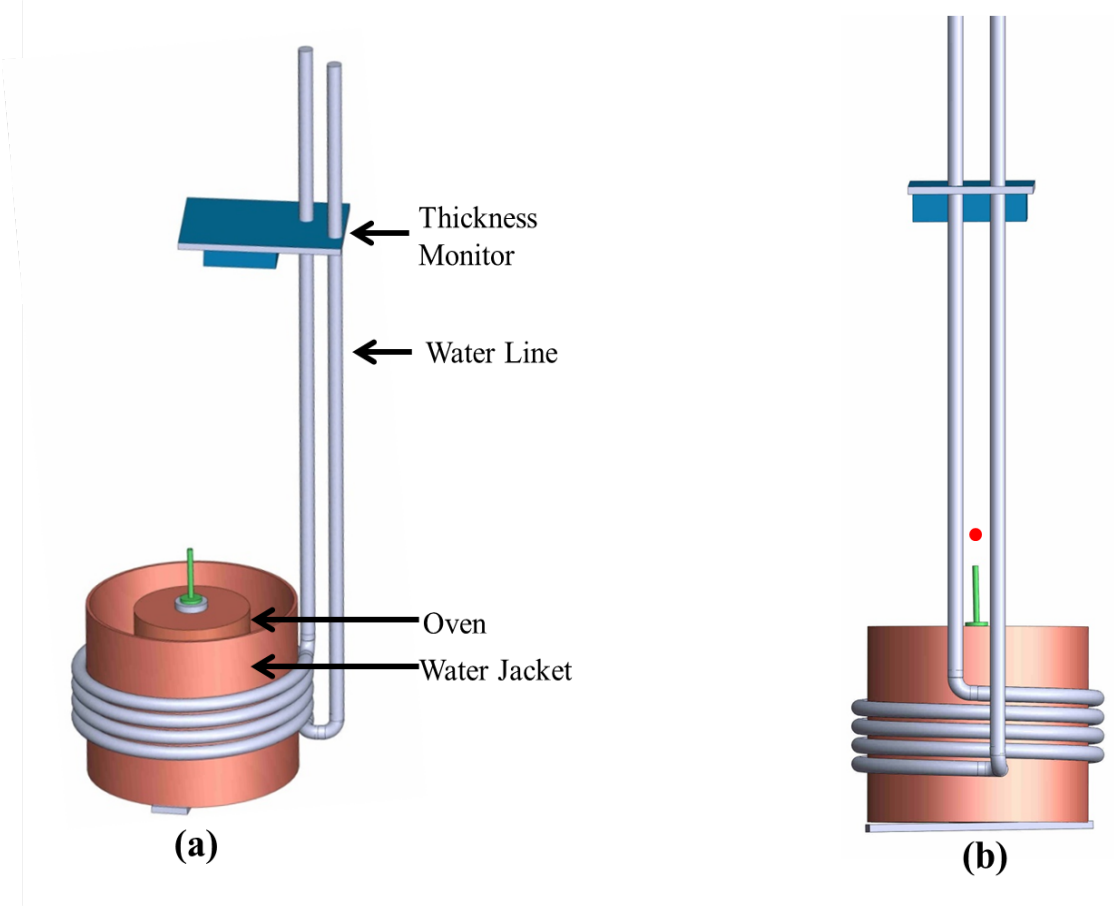

Figure 2.6: 3-D mechanical drawing of the oven assembly (made using SolidWorks-2014); (a) side view, along the beamline (b) view perpendicular to the beamline, red spot showing the beam perpendicular to the plane of the paper.

Further, it is extremely important to obtain a steady flow of the vapour while performing the measurements. The density of the vapour effusing out of the nozzle is highly sensitive to the temperature fluctuations (if any) in the metallic oven. To monitor the density fluctuations, a quartz crystal based thickness monitor (INFICON SQM 160 Multi-Film Rate/Thickness monitor) was mounted above the nozzle. The crystal is excited into mechanical motion by an external oscillator. The unloaded crystal oscillates in thickness shear mode at a certain frequency. As the evaporating material is deposited on the crystal, the frequency of oscillation changes and this change in frequency is proportional to the mass of the deposited film. To ensure a steady and gradual increase of the flow rate, the temperature of the oven was increased very slowly, i.e., approximately 24 hrs was devoted for reaching the desired temperature which eventually gave a decent flow rate for performing the experiment. The rate of flow of the effusing vapour of bromouracil was noted throughout the experiment. Figure 2.7 shows the rate of flow of the vapour as a function of time. It is seen that the rate (plotted in angstrom/sec) remains uniform over a period of 7 hrs. Data was collected only after ensuring a uniform flow of the vapour.

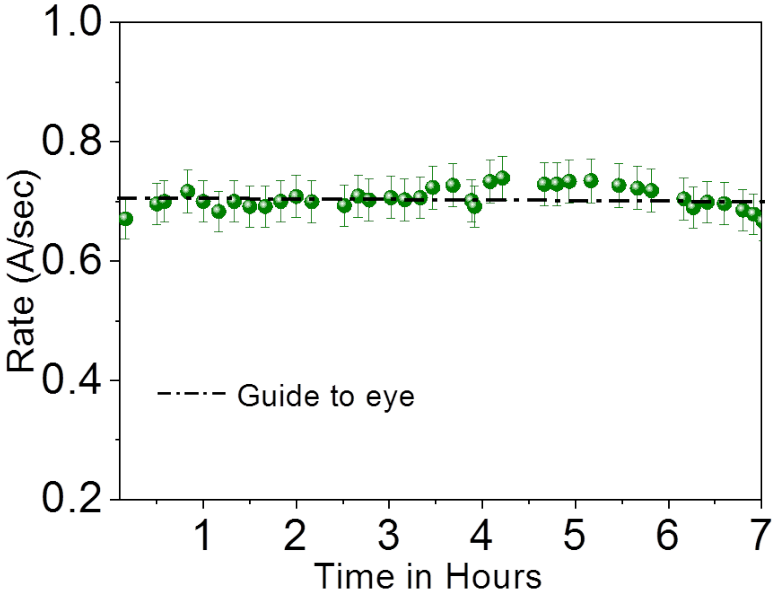

Figure 2.7: Rate of flow of evaporated bromouracil as a function of time.

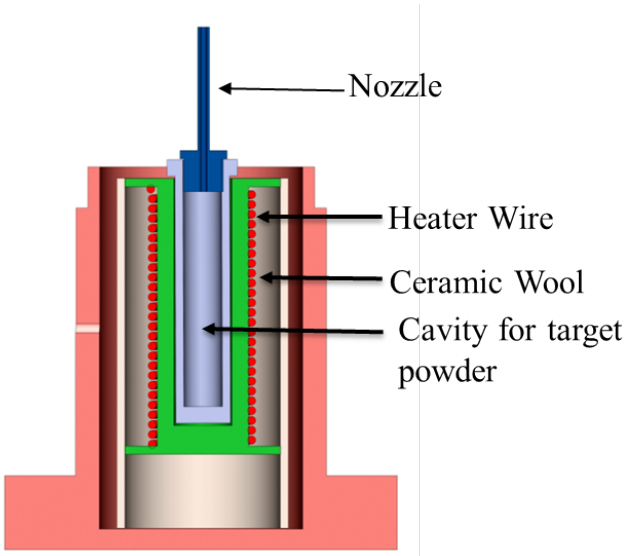

Figure 2.8: Mechanical drawing of the oven showing all the different parts (cross sectional view).

Similar procedure was also followed for uracil target.

The metallic oven along with the powder holder and nozzle, water jacket with the water tubing and the thickness monitor were all made as part of a single target holder assembly which was connected to a 3D translation stage manipulator for proper alignment of the target vapour with the projectile beam. Figure 2.9 displays the target holder assembly that was used for the present experiments. This assembly was designed and fabricated for this thesis work.

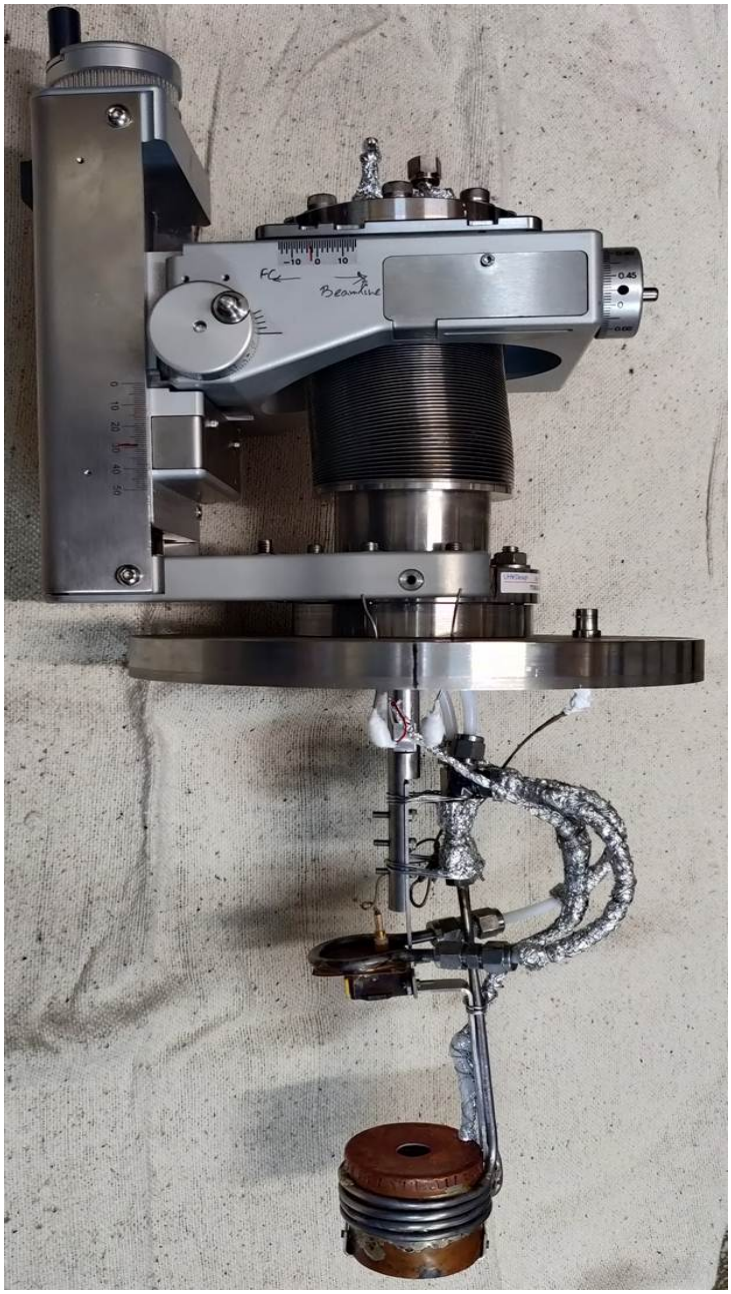

Figure 2.9: Target holder assembly connected to XYZ stage manipulator.

2.2.6 Electron Spectrometer

The electrons ejected from the target in the collision process were energy analyzed by the hemispherical electrostatic analyzer sitting on the turntable. Figure 2.10 shows the cut view of the spectrometer. The inner and outer electrodes of the analyzer and it's housing were all made of OFHC copper. The inner and outer hemispheres have diameter 25 mm and 35 mm, respectively. The analytical relationship between the electron energy and applied voltages to

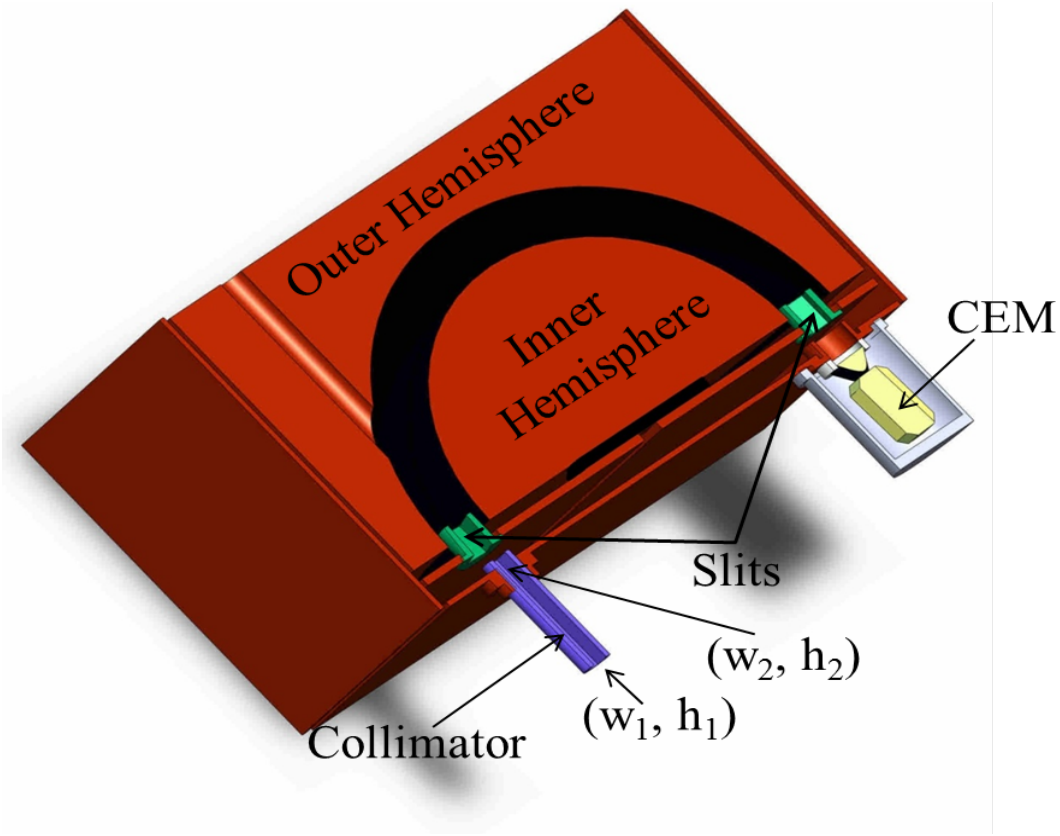

Figure 2.10: 3-D mechanical drawing of the cutaway view of the electron spectrometer (made using SolidWorks-2014).

the electrodes is given by

$$HV_1 = (V_c + \epsilon_e)\frac{R_2 - R_1}{R_1} + V_c \tag{2.1}$$

$$HV_2 = -(V_c + \epsilon_e)\frac{R_2 - R_1}{R_2} + V_c \tag{2.2}$$

where R_1 and R_2 are the radii of the inner and outer hemispheres, respectively and ϵ_e denotes the energy of the electron being scanned. These equations are obtained by solving the Laplace's equation, $\nabla^2 V(r) = 0$ in spherical polar coordinates with the boundary conditions, $V(R_1) = HV_1$ and $V(R_2) = HV_2$. V_c denotes the pre-acceleration voltage which is a small positive voltage of few volts, applied to the entrance and exit slits of the spectrometer to increase the collection efficiency of the low energy electrons ($\leq$ 5 eV), which are otherwise very difficult to detect. These low energy electrons get deflected easily due to any stray field near the interaction region. Depending on the biasing of the electrodes, electrons of a definite energy will pass through the exit slit whereas the other electrons will hit the electrodes. These electrons can further produce a large number of secondary electrons from the surface of the electrodes which can eventually contribute to a large background in the electron spectrum. In order to reduce

this background, the curved surfaces of the electrodes were coated with carbon soot which helps in diminishing the secondary electron emission. Two rectangular apertures were placed at the beginning (w_1, h_1) and end (w_2, h_2) in Figure 2.10 of the extended collimator which was connected to the entrance of the analyzer. The effect of the pre-acceleration voltage (V_c) on the spectrometer collection efficiency was studied by recording the electron count rate as a function of V_c.

The analyzer energy resolution depends mostly on the exit slit width and the acceptance angle of the entrance slit. The resolution of the analyzer can be analytically written as

$$R = \frac{\Delta\epsilon}{\epsilon_0} = \left(\frac{x_1 + x_2}{R_1 + R_2}\right) + \alpha^2 \tag{2.3}$$

where, x_1 and x_2 are the deviations from the object point and the image point respectively, and α is the acceptance angle of the analyzer. The measured energy resolution of the analyzer is given by (FWHM/ϵ_0). For FWHM, the value of $(x_1 + x_2)$ becomes equal to the larger slit width. The acceptance angle α is determined by the collimating slit geometry in front of the entrance slit of the analyzer. The resolution of the analyzer was found to be $\sim 6\%$. In case of flooded chamber experiment, the entire scattering chamber is filled with the target gas (at a definite static pressure) and hence the collision volume extends along the electron/ion beam. In such situation, the acceptance angle of the analyzer varies between 3.4^0 to 3.6^0 depending on the emission angle. The corresponding estimated average uncertainty in electron emission angle is about 3.5^0. The contribution from α is 1% of the energy resolution of the analyzer of 6%. This analyzer was used for performing experiments with the electron gun assembly and for experiments with the Pelletron accelerator.

In case of the scattering chamber connected to the 50^0 north beamline at ECRIA, another hemispherical electrostatic analyzer was mounted, which was almost identical to the above mentioned analyzer. The radii of the hemispheres were similar (i.e., 25 and 35 mm). The rectangular apertures at the two ends of the extended collimator (w_1, h_1 and w_2, h_2 in Figure 2.10) of the spectrometer had slightly varying dimensions. We have tabulated these values for the two analyzers used in the present thesis work in table

2.2.7 Detector

A channel electron multiplier (CEM) was used to detect the energy analyzed electrons. When an electron strikes the front of the CEM, it typically produces few secondary electrons. These electrons are further accelerated by the applied positive bias and strike the channel walls, producing enormous secondary electrons. The resulting avalanche process produces an output pulse of charge containing around $10^7 - 10^8$ electrons within a time duration of about 8 nanoseconds. The detection efficiency of CEM (electron counting mode) is maximum ($0.87 \pm 10\%$) in the energy range of $100 - 600$ eV, obtained from the operation manual of the detector [56]. Thus the front cone of the CEM was kept at a positive potential of 100 V for all the experiments

to have maximum efficiency for electron detection. The back of the CEM was kept at $+2500$ Volt, thus maintaining a constant voltage difference of +2400 Volts between the front and back of the CEM. Figure 2.11 shows the schematic of the biasing circuit for the CEM in electron counting mode. Figure 2.12 shows the picture of a typical CEM output pulse.

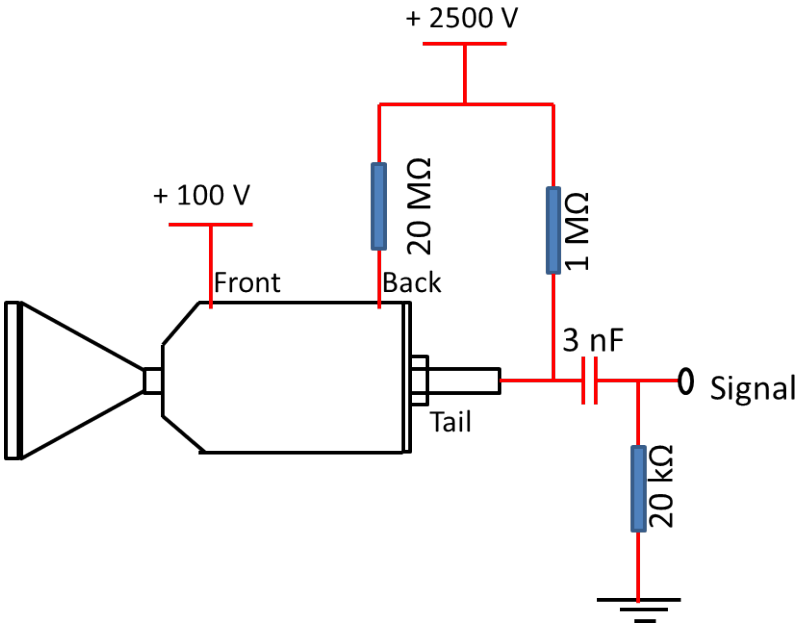

Figure 2.11: CEM biasing circuit

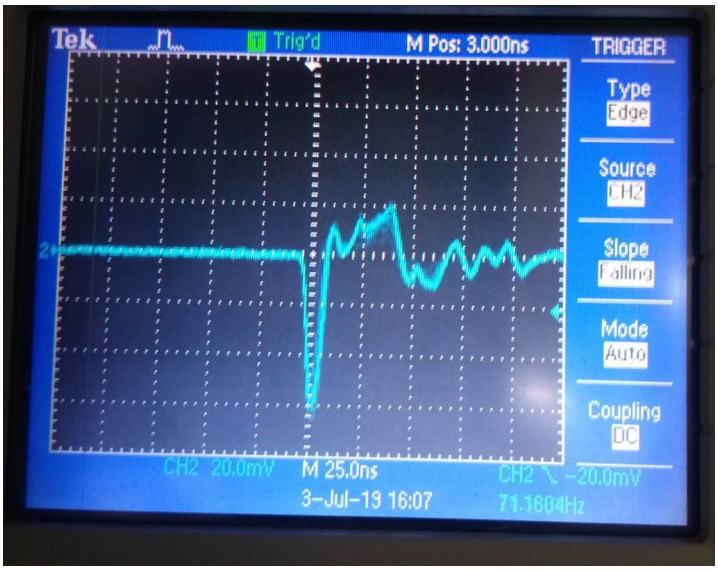

Figure 2.12: CEM output pulse.

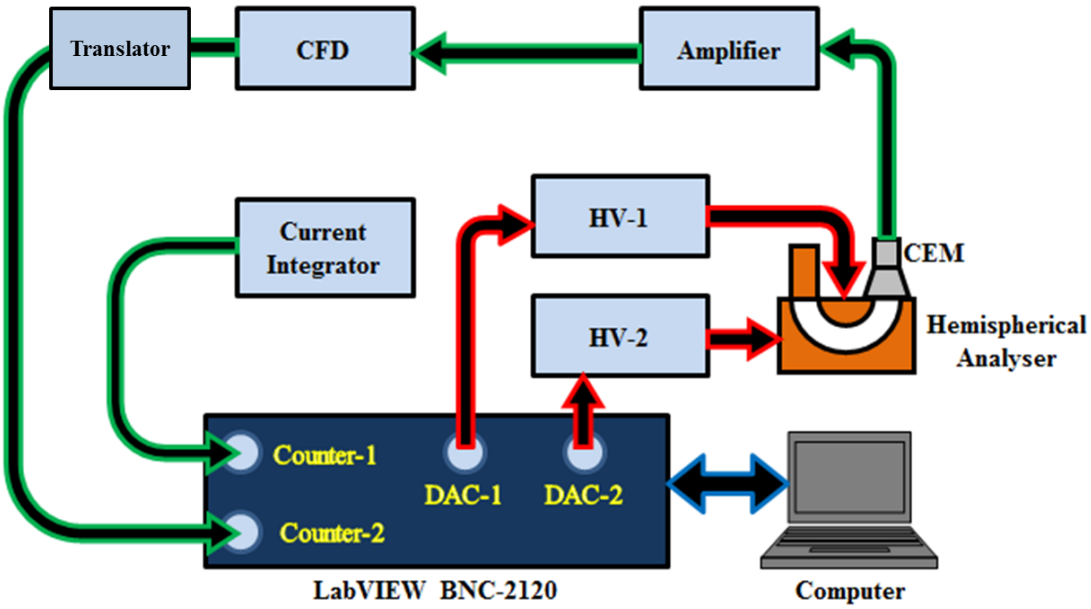

Figure 2.13: Schematic diagram of the data acquisition system

2.2.8 Data Acquisition System

Figure 2.13 shows the schematic diagram of the data acquisition system. The electrons of a definite energy were scanned by applying appropriate voltages on the electrodes. The voltages on the electrodes were scanned remotely from a computer via a LabVIEW based software interface. The energy analyzed electrons were then detected by the CEM, sitting at the exit slit of the spectrometer. The analog signal from the CEM was fed to a timing filter amplifier (TFA) which was then followed by a constant fraction discriminator (CFD). The CFD produces a NIM pulse which is then fed to the translator that finally generates the TTL pulse. The CFD produces a pulse only if the input analog pulse from CEM has an amplitude exceeding the applied threshold level. The digital pulse from the translator is fed directly to the LabVIEW counter. At each energy, the number of electrons ejected were detected for a specified amount of incident projectile charge collected on the Faraday cup. The Faraday cup was connected to a digital current integrator, the output of which was in turn fed into the LabVIEW counter (see Figure 2.13).

2.3 Testing of the spectrometer

Some of the basic parameters were tested before actual data collection. The pre-acceleration voltage (V_c) was increased and correspondingly the electron count rate was checked at every instance. Figure 2.14 shows the change in count rate of the low energy electrons as a function of V_c. It is clearly seen that a selection of 6 V is sufficient to increase the collection of low

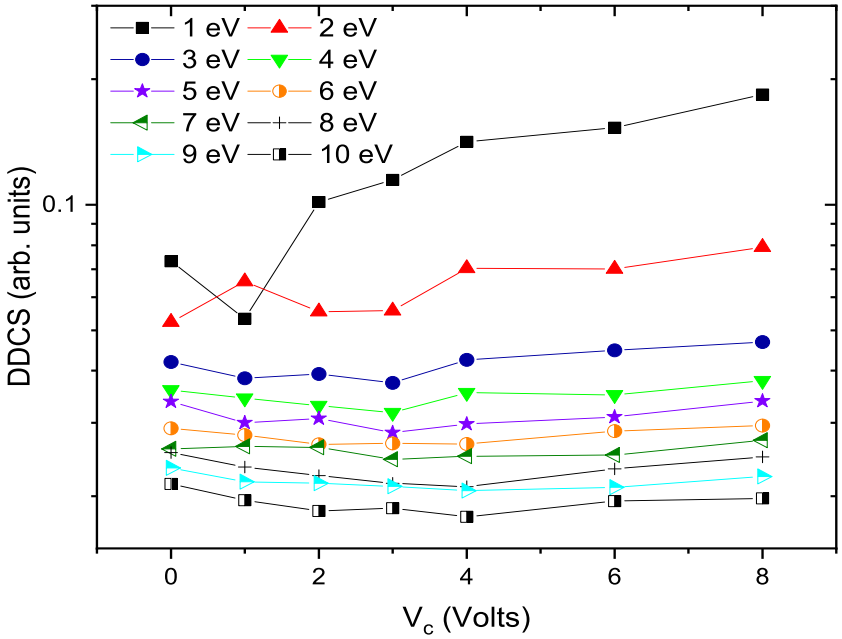

Figure 2.14: Variation of count rate with change in pre-acceleration voltage.

energy electrons. Thus V_c = 6 V was used for the different set of experiments.

Figure 2.15 display the topview of the scattering chamber housing the turntable and the spectrometer. In Figure 2.15(a), some of the focussing elements are seen to be in close proximity to the spectrometer. The other side of these elements are connected to the electron gun assembly (not shown in this figure). Figure 2.3 shows the entire picture of the e-gun beamline, scattering chamber along with the deflectors and lens protruding inside the scattering chamber. Due to the close proximity of the deflectors and lens to the spectrometer, they were covered with a non-magnetic stainless steel cap (shown in Figure 2.15(b)) to avoid penetration of electric field into the interaction zone, which could deflect the ejected electrons. However, several tests were performed to ensure that there was no field effect near the interaction region due to these focussing elements. For this purpose, for a given electron beam energy, different voltages were applied on the Einzel lens and deflectors and correspondingly the count rate was checked at every instant. The Einzel lens voltage was approximately few kV whereas that applied on the deflectors was around 100 V. Figure 2.16 shows the DDCS spectra collected for 7 keV e^- impact on N_2 at different combinations of lens and deflector voltages. The spectra were collected upto 100 eV for each case and it is seen that beyond 20 eV, they tend to merge together.

The dispersion in the count rate is seen to occur only for the low energy electrons. It is clearly observed that in spite of covering the focussing elements with the cap, higher lens voltages resulted in decreasing count rate for the lowest energy electrons. The yield of 3 eV electrons as a function of lens voltage is shown in the inset. For 7 keV impact energy, the

(a)

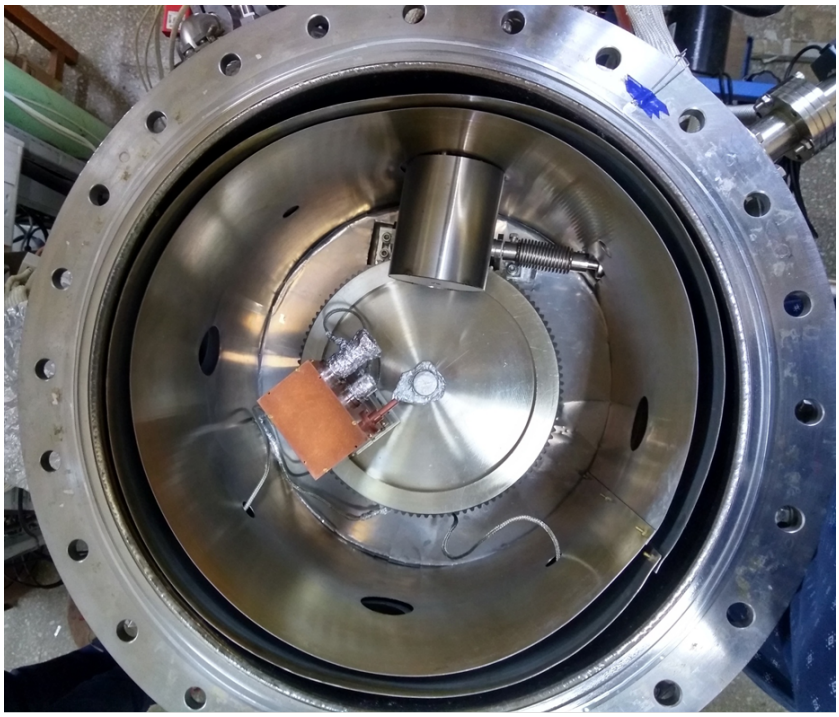

(b)

Figure 2.15: Scattering chamber seen from top along with turntable and spectrometer: (a) X-Y deflectors close to the spectrometer and (b) deflectors covered with non-magnetic stainless steel cap. Two layers of thin μ metal sheets are seen at the circumference of the chamber.

combination of Einzel lens voltage at 1.5 kV with the deflector voltages "ON" (blue solid triangles) was selected for the electron beam optimization. Any combination of voltages higher

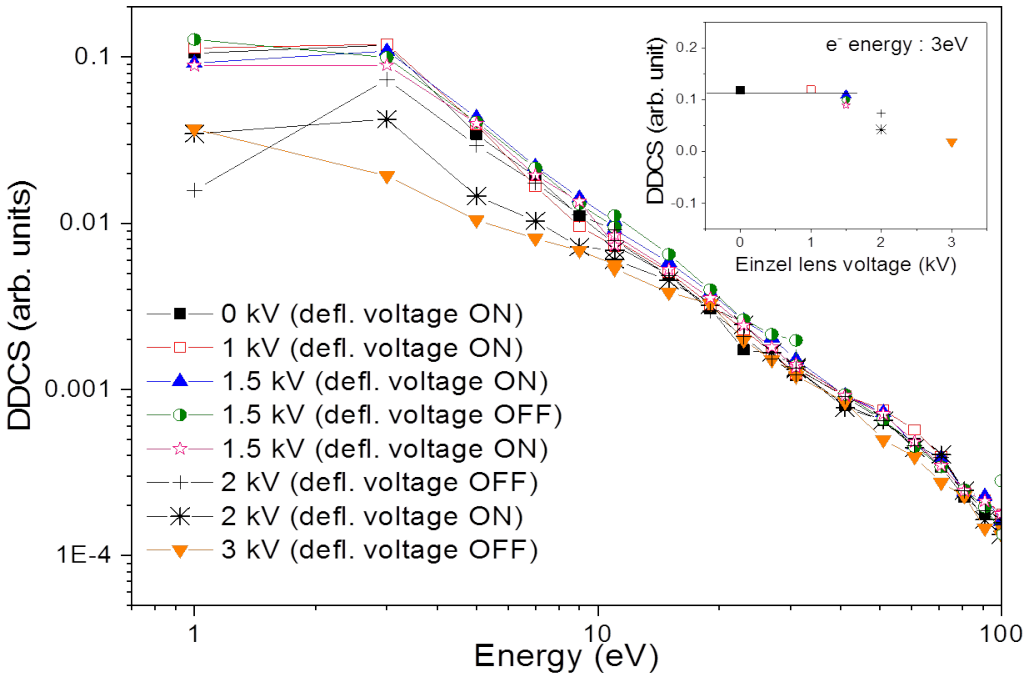

Figure 2.16: DDCS spectra for 7 keV e^- impact on N_2, collected for different combinations of lens and deflector voltages. Inset : Variation of count rate for 3 eV electrons as a function of Einzel lens voltage.

than these resulted in decrease of count rate, whereas tuning the 7 keV electron beam for lens voltages less than 1.5 kV (in the present geometry, discussed in section 1.2.3) was an extremely difficult task and lead to poor beam quality.

Further, the DDCS for elastic scattering of electrons in case of 2 keV electron impact on N_2 were measured for different forward and backward emission angles. The single differential cross-sections ($d\sigma/d\Omega$) have been deduced from the DDCS by integrating it numerically over the emission energy. Figure 2.17 display the SDCS of elastic scattering as a function of emission angles. The dashed line shows the $cosec^4(\theta/2)$ dependence which is scaled appropriately. The data matches quantitatively well with the prediction of the Rutherford's well known formalism for elastic scattering. This test provided a convincing check on the performance of the spectrometer.

2.4 Theory of Measurement

The double differential cross sections at a given emission angle, were obtained from the number of electrons detected in presence and absence of the target gas given by the relation

$$\frac{d^2\sigma}{d\epsilon d\Omega} = \frac{\frac{N_e(\epsilon,\theta)}{N_p \Delta\epsilon} - \frac{N_b(\epsilon,\theta)}{N'_p \Delta\epsilon}}{n\epsilon_{el}(l\Omega)_{eff}} \tag{2.4}$$

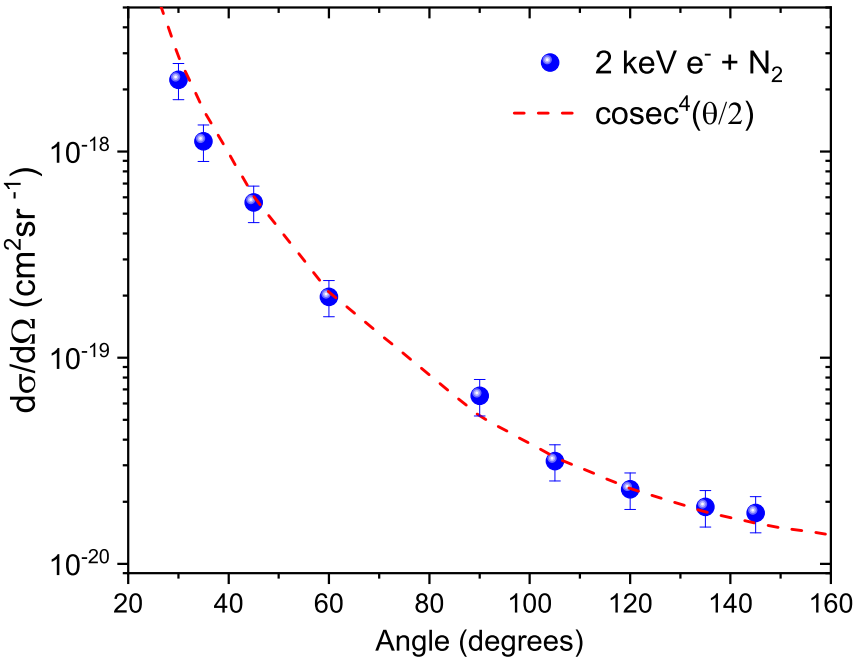

Figure 2.17: Single differential cross section of elastic scattering for 2 keV electron impact on N_2. Solid line corresponds to the Rutherford formula of elastic scattering fitted to the experimental data.

where N_e represents the number of electrons detected in the presence of the target gas corresponding to N_p number of projectile electrons/ions
Similarly, N_b is the number of background counts corresponding to N'_p number of projectile electrons/ions
n = 9.659 x $10^{15} P_c(mTorr)/T(K)$ is the target number density under static gas pressure condition
$\Delta\epsilon = 0.06(\epsilon + V_c)$ is the energy resolution of the spectrometer
ϵ_{el} is the detection efficiency of the detector (CEM) and
$(l\Omega)_{eff}$ is the solid angle path length integral which is given by

$$(l\Omega)_{eff} = \frac{w_1 w_2 h_2}{LRsin(\theta)} \tag{2.5}$$

where w_1, w_2 and h_2 are the widths and height of the rectangular apertures at the front and back of the spectrometer collimator (see Figure 2.10), L is the length of the collimator and R is the distance of the collimator from the center of the interaction region. The dimensions of these apertures along with the length L and distance R corresponding to the two spectrometers used for the present series of experiments are tabulated below :

From Figure 2.3 it is seen that the spectrometer sits on a base plate on the turn table. There

Table 2.1: Specifications of the spectrometer collimators, all dimensions are in mm

Spectrometer	w_1	h_1	w_2	h_2	L	R
Spectrometer for Pelletron	3	4	2	3	36.5	59.5 on second slot of base plate
Spectrometer at ECRIA	4	4	3	4	36.1	57.4 on first slot of base plate

are two slots on the base plate for the setup used at Pelletron and electron gun, whereas three slots for the one used at the experimental setup connected to the 50^0 north beamline at ECRIA. The value of R changes with respect to the slot on which the spectrometer sits and hence $(l\Omega)_{eff}$ changes accordingly. For a particular value of R, $(l\Omega)_{eff}$ is least and 90^0 and increases for other scattering angles.

In case of an effusive jet source, the solid angle path length integrand has to be convoluted with the molecular jet density distribution profile, whose variation as a function of spread angle at a given distance from the nozzle tip is given by [57]

$$j(\phi) = \alpha cos\phi + \frac{2}{\pi} cos\phi \Big[(1-\alpha)R(q) + \frac{2}{3q}(1-2\alpha)\{1-(1-q^2)^{3/2}\} \Big] \tag{2.6}$$

for $q \leq 1$ and

$$j(\phi) = \alpha cos\phi + \frac{4}{3\pi q}(1-2\alpha) cos\phi \tag{2.7}$$

for $q \geq 1$ where

$$R(q) = cos^{-1}q - q(1-q^2)^{1/2} \tag{2.8}$$

$q = \frac{tan\phi}{\beta}$, where $\beta = \frac{2r}{L}$ is the aspect ratio of the jet nozzle and

$$\alpha = \frac{1}{2} - \frac{1}{3\beta^2} \Big[\frac{1-2\beta^2 + (2\beta^2-1)(1+\beta^2)^{1/2}}{(1+\beta^2)^{1/2} - \beta^2 sinh^{-1}(\frac{1}{\beta})} \Big] \tag{2.9}$$

The effective solid angle path length is given by :

$$(l\Omega)_{eff} = \int_Z \Omega(\theta, z) j(z) dz \tag{2.10}$$

From Figure 2.18 it is seen that z assumes the values from Z_1 to Z_4, defined as follows :

$$Z_1 = -(R-d)\frac{sin\epsilon}{sin\rho} \tag{2.11}$$

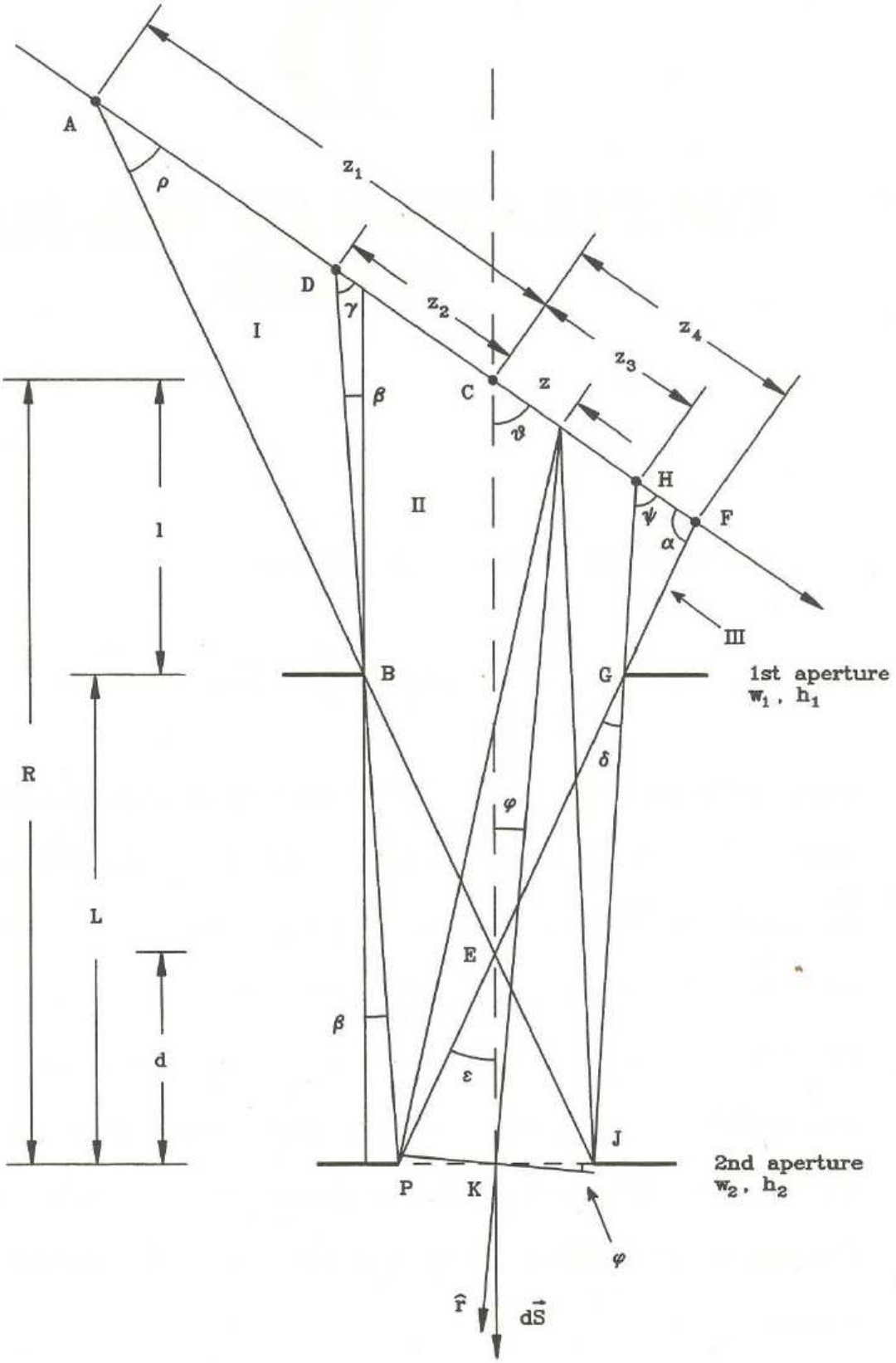

Figure 2.18: Solid angle geometry for the calculation of path length integral (Taken from [58])

$$Z_2 = -\Big[\frac{sin\beta}{sin\gamma}(l + \frac{1}{2}w_1 cot\theta) + \frac{w_1}{2sin\theta}\Big] \tag{2.12}$$

$$Z_4 = (R - d)\frac{sin\epsilon}{sin\alpha} \tag{2.13}$$

$$Z_3 = Z_4 - \frac{sin\delta}{sin\psi sin\epsilon}(Z_4 sin\theta - \frac{1}{2}w_1) \tag{2.14}$$

where,

$$tan\epsilon = \frac{w_1 + w_2}{2L} \tag{2.15}$$

$$tan\beta = \frac{w_1 - w_2}{2L} \tag{2.16}$$

$$\delta = \epsilon - \beta \tag{2.17}$$

$$\rho = \theta - \epsilon \tag{2.18}$$

$$\gamma = \theta - \beta \tag{2.19}$$

$$\alpha = (180^0 - \theta - \epsilon) \tag{2.20}$$

$$\psi = \theta + \beta \tag{2.21}$$

Now, in **Region II** of Figure 2.18, $\Omega(\theta, Z)$ is given by :

$$\Omega(\theta, Z) = \frac{w_2 h_2 (R - Z cos\theta)}{(R^2 + Z^2 - 2ZR cos\theta)^{3/2}} \tag{2.22}$$

In **Region I and III**, $\Omega(\theta, Z)$ is expressed as :

$$\Omega(\theta, Z) = \frac{(w_2 - u)h_2 cos\phi}{(R \pm Z cos\theta)^2 + (\frac{u}{2} + Z sin\theta)^2} \tag{2.23}$$

where

$$cos\phi = \frac{R - \nu \pm Z cos\theta}{\sqrt{(R - V \pm Z cos\theta)^2 + (Z sin\theta)^2}} \tag{2.24}$$

$$\nu = u\frac{R \pm Z sin\theta}{u + 2Z sin\theta} \tag{2.25}$$

$$u = \frac{L}{l \pm Z cos\theta}\Big[Z sin\theta - \frac{w_1}{2} - (l \pm Z cos\theta) tan\beta\Big] \tag{2.26}$$

2.5 Summary

To summarize, we have used the electron spectroscopy technique to measure the DDCS of the electrons emitted from target atoms/molecules in collisions with projectile ions and electrons. The experiments have been performed using the 14 MV Pelletron accelerator, 14.5 GHz ECR ion accelerator and the keV energy electron gun. The accelerating column of the ECRIA and the 50^0 N beamline (dedicated for electron spectroscopy) were realigned with respect to the ion source before performing the experiments. The beamline for electron gun assembly was also revamped for carrying out the experiments. The electron spectrometer was characterized and it's performance was tested by carrying out different test measurements. An oven assembly, connected to a 3D translation stage manipulator was built for the present thesis work. This oven assembly was used for preparing vapour from the powders of uracil and bromouracil .